

Schwarps: Locally Projective Image Warps

Based on 2D Schwarzian Derivatives

Daniel Pizarro

Rahat Khan

Adrien Bartoli

ISIT, UMR 6284 CNRS-UdA

Clermont-Ferrand, France

Corresponding author: Rahat Khan

`rahatkhanr@gmail.com`

November 4, 2014

Abstract

Image warps -or just warps- capture the geometric deformation existing between two images of a deforming surface. The current approach to enforce a warp's smoothness is to penalize its second order partial derivatives. Because this favors locally affine warps, this fails to capture the local projective component of the image deformation. This may have a negative impact on applications such as image registration and deformable 3D reconstruction. We propose a novel penalty designed to smooth the warp while capturing the deformation's local projective structure. Our penalty is based on equivalents to the Schwarzian derivatives, which are projective differential invariants exactly preserved by homographies. We propose a methodology to derive a set of Partial Differential Equations with only homographies as solutions. We call this system the Schwarzian equations and we explicitly derive them for 2D functions using differential properties of homographies. We name as Schwarp a warp which is estimated by penalizing the residual of Schwarzian equations. Experimental evaluation shows that Schwarps outperform existing warps in modeling and extrapolation power, and lead to better results in three deformable reconstruction methods, namely, shape reconstruction in Shape-from-Template, camera calibration in Shape-from-Template and Non-Rigid Structure-from-Motion.

Keywords— Schwarzian Penalizer, Bending Energy, Projective Differential Invariants, Image Warps

Contents

1	Introduction	3
2	State-of-the-Art	6
3	Background	7
3.1	The Cross-Ratio	7
3.2	The 1D Schwarzian Derivative	8
3.3	Multidimensional Schwarzian Derivatives (MSDs)	8
4	Schwarzian Equations in Two Dimensions	9
4.1	The 1D Schwarzian Derivative	9
4.2	The 2D Schwarzian Equations	10
5	Solution Space of the Schwarzian Equations	12
5.1	Solution Space of the 1D Schwarzian Derivative	12
5.2	Solution Space of the 2D Schwarzian Equations	13
6	Modeling the Perspective Projection of Deforming Surfaces: Schwarzps	15
7	Experimental Results	17
7.1	Implementation Details	17
7.2	Synthetic Data	17
7.2.1	Effect of Noise and Hyperparameter	18
7.2.2	Effect of Perspective	19
7.2.3	Effect of Deformation	19
7.2.4	Rate of Convergence	19
7.3	Real Data	20
7.3.1	Shape Reconstruction in Shape-from-Template	21
7.3.2	Calibration in Shape-from-Template	21
7.3.3	Non-Rigid Structure-from-Motion	22
8	Conclusion	24

1 Introduction

Projective geometry studies the geometric properties of projective transformations. During the last 30 years, projective geometry has successfully modeled important problems in computer vision, such as image stitching (Szeliski, 2006), image registration (Torr, 2000) and Structure-from-Motion (SfM) (Faugeras et al., 2001; Hartley and Zisserman, 2003). These problems assume the scene is rigid. However, if the scene geometry changes over time, the current tools from projective geometry cannot model it. They are thus insufficient for problems like Non-Rigid Structure-from-Motion (NRSfM) (Bregler et al., 2000; Torresani et al., 2008), Shape-from-Template¹ (SfT) (Perriollat et al., 2011; Salzmann et al., 2007) and non-rigid image registration (Bookstein, 1989). In a deformable environment, a fundamental problem is the modeling of the image warp -or just warp- the function which maps points between images of a deforming surface. A warp is generally represented by a linear basis expansion such as the Thin-Plate Spline (TPS) (Bookstein, 1989), the tensor-product BSpline (BS) (Rueckert et al., 1999), finite elements (Pilet et al., 2007) and finite differences as in optical flow (Horn and Schunck, 1981). A warp is also generally assumed to be smooth or piecewise smooth. This is modeled by existing approaches as a penalty on the warp’s derivatives. For instance, penalizing second order derivatives leads to the popular bending energy, which forces the warp to be locally affine (Bookstein, 1989). A direct consequence is that the infinitesimal projective information is not captured by the warp. Interestingly, it was attempted to solve that problem by modeling the warp with rational basis expansion. This led to the Generalized TPS warps (Bartoli et al., 2010) and the NURBS warp (Brunet et al., 2009). Their estimation uses the 3D bending energy directly expressed on homogeneous coordinates. Theoretically, rational warps are smooth and capture the infinitesimal projective structure. However, their main problem is that they are non-convex and may be unstable due to their rational structure.

We propose a novel penalty which is able to smooth a warp while allowing it to capture the infinitesimal projective structure. This penalty may be used to estimate *any* type of warp model. Therefore, it may be applied to linear basis expansions, and does not require the use of a rational warp. Our penalty is based on the theory of Projective Differential Geometry (PDG), which we argue is a fundamental tool in warp modeling. PDG is a branch of mathematics that studies the properties of projective transformations at the infinitesimal scale. So far, PDG has been used to a much smaller extent than projective geometry in computer vision (Lazebnik and Ponce, 2005; Schmid and Zisserman, 2000). An important result of PDG is the Schwarzian derivative (Ovsienko and Tabachnikov, 2009). It originated from the study of projective

¹In SfT, the 3D shape of a deformable surface is computed from the warp between a template and an input image. The shape of the template is known a priori.

differential invariants, but also appears in many other fields of mathematics such as the dynamical system theory and differential equation solving. The Schwarzian derivative models cross-ratio at a differential level (Ovsienko and Tabachnikov, 2009). The cross-ratio of points is well-known in computer vision (Lei, 1990; Mundy and Zisserman, 1992) as it represents a projective invariant between two images related by a homography. In \mathbb{RP}^1 , the cross-ratio is defined for 4 colinear points. In the differential cross-ratio the distances among these points are infinitesimal. The Schwarzian derivative is a differential operator that vanishes for functions that preserve the differential cross-ratio. The Schwarzian derivative is well defined in the 1D case (Ovsienko and Tabachnikov, 2009; Singer, 1978). However, we are interested in images and thus in the 2D case. Several extensions of the Schwarzian derivative to higher dimensions were proposed (Matsumoto et al., 1993; Osgood and Stowe, 1992; Ovsienko and Tabachnikov, 2005). Computing the Schwarzian derivatives of an image warp requires one to find a system of PDEs that, as in the case of the 1D Schwarzian derivative, has homographies as solutions. Unfortunately, it is far from straightforward to arrive from the existing multidimensional Schwarzians to the sought system of PDEs (see section 3.3 for details).

We bring two core contributions. The first one is a new derivation framework for the 1D Schwarzian derivative which extends to higher dimensions. In particular, we use our framework to explicitly derive a system of PDEs that we call the *2D Schwarzian equations*. Interestingly, the 2D Schwarzian equations are second order PDEs contrary to the third order 1D Schwarzian derivatives. Our second core contribution is the *Schwarz*, which is defined as an image warp which was estimated while penalizing the residual of our 2D Schwarzian equations, thereby capturing infinitesimal projective properties. The intuition underlying this penalizer is that a warp with small residuals for our 2D Schwarzian equations behaves locally like a homography. To back this intuition, we prove that the 2D Schwarzian equations vanish if and only if the warp is a homography. A Schwarz may be constructed with any warp model and improves over classical approaches based on using the bending energy as a penalizer, favoring a locally affine behavior (see figure 1).

We report an extensive set of experimental results. Schwarzs do better than state-of-the-art warps in three ways: *(i)* the warp’s extrapolation power increases, especially in perspective imaging conditions, *(ii)* the accuracy of the warp’s derivatives is improved by a large margin, *(iii)* the sensitivities to the hyperparameter is reduced. We validated the impact of Schwarzs on three methods: shape reconstruction in SfT (Bartoli et al., 2012), camera calibration in SfT (Bartoli and Collins, 2013b) and NRSfM (Varol et al., 2009).

Notation. We briefly discuss our notation. Lowercase greek letters (e.g. γ) are functions, functionals or parameters. Scalars are latin lowercase letters in italics (e.g. n). Latin uppercase letters in italics are used for differential operators (e.g. S) except J which denotes the Jacobian determinant. \mathbb{R}^n and \mathbb{RP}^n denote respectively the real vector space and the real projective space of dimension n . Calligraphic letters are used

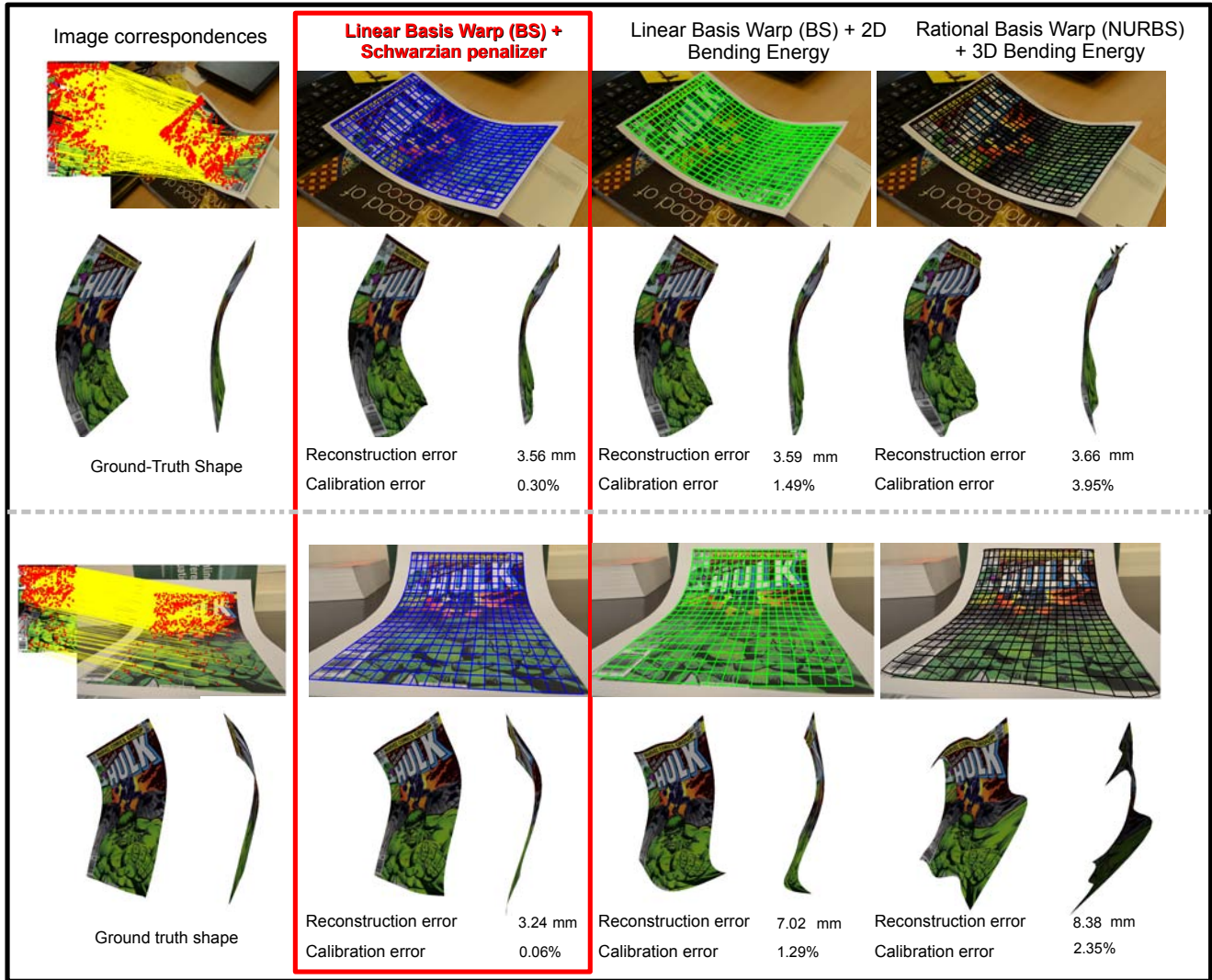


Figure 1: Shape-from-Template (SfT) results for different warp models. In these examples, the BS-warp is used as the linear basis warp and the NURBS-warp as the rational basis warp. The first column shows the input feature correspondences and the ground truth shape obtained by SfM for multiple images. The image in the first row is captured under affine conditions whereas the image in the second row is significantly perspective. It is clear that the warp that uses Schwarzian equations as a penalizer improves accuracy over the other warps in both cases. However, in the presence of strong perspective the gain is significant. SfT depends on the first derivative of the warp which is captured with our penalizer to a better extent than with the usual bending energy. The shape reconstruction in SfT method we used is (Bartoli et al., 2012) and the calibration in SfT method is (Bartoli and Collins, 2013a)

to define groups of functions under composition. We denote as $\mathcal{L}(\mathbb{R}^n)$ the group of linear functions in n dimensions with scalar range. Given $\gamma \in \mathcal{L}(\mathbb{R}^n)$ and x_i the i -th input variable, we have that:

$$\frac{\partial^n \gamma}{\partial x_i} = 0 \quad n > 1 \quad i \in \{1, \dots, n\}. \quad (1)$$

We denote as $\mathcal{A}(\mathbb{R}^n)$ the group of affine transformations, where given $\eta \in \mathcal{A}(\mathbb{R}^n)$:

$$\eta = \left(\gamma_1 \quad \gamma_2 \quad \dots \quad \gamma_n \right)^\top \quad \gamma_i \in \mathcal{L}(\mathbb{R}^n) \quad \text{and} \quad i \in \{1, \dots, n\}. \quad (2)$$

We denote as $\mathcal{H}(\mathbb{R}\mathbb{P}^n)$ the group of homographic functions, defined using ratios of members of $\mathcal{L}(\mathbb{R}^n)$. Given $\eta \in \mathcal{H}(\mathbb{R}\mathbb{P}^n)$:

$$\eta = \left(\frac{\delta_1}{\delta_{n+1}} \quad \frac{\delta_2}{\delta_{n+1}} \quad \dots \quad \frac{\delta_n}{\delta_{n+1}} \right)^\top \quad \delta_i \in \mathcal{L}(\mathbb{R}^n) \quad i \in \{1, \dots, n+1\} \quad \text{and} \quad \delta_{n+1} \neq 0. \quad (3)$$

Finally, we denote $\mathcal{C}^r(\mathbb{R}^n, \mathbb{R}^n)$ the group of continous functions that have continuous first r derivatives.

2 State-of-the-Art

We provide some details on the existing warps and the penalty used for imposing smoothness, a very important prior when estimating image warps. The warps discussed here are later compared to ours in the experimental section. The most commonly used warps are the linear basis expansion warps which are usually obtained as the optimum of a linear least-square problem of the following form:

$$\arg \min_{\eta} \quad \varepsilon_d[\eta] + \lambda \varepsilon_s[\eta], \quad (4)$$

where η is the warp, $\varepsilon_d[\eta]$ is the data term and $\varepsilon_s[\eta]$ is the penalty term which smoothes the warp. λ is a *hyperparameter* that determines the weight of the penalty. Typically, the bending energy $\varepsilon_{be}[\eta]$ is used as penalty:

$$\varepsilon_s[\eta] = \varepsilon_{be}[\eta] = \int_{\mathbb{R}^2} \left(\frac{\partial^2 \eta}{\partial u^2} \right)^2 + \left(\frac{\partial^2 \eta}{\partial u \partial v} \right)^2 + \left(\frac{\partial^2 \eta}{\partial v^2} \right)^2 \quad dudv, \quad (5)$$

where u and v are the domain coordinates of the warp. Imposing hardly the bending energy to be zero forces the warp to be an affine transformation:

$$\lim_{\lambda \rightarrow \infty} \left(\arg \min_{\eta} \quad \varepsilon_d[\eta] + \lambda \varepsilon_{be}[\eta] \right) \quad \in \quad \mathcal{A}(\mathbb{R}^2). \quad (6)$$

Any warp model, such as the TPS-warp or the BS-warp that uses the bending energy to impose smoothness fails to capture perspective at a differential level. To deal with that problem, warps based on rational basis expansions were proposed. For example, (Bartoli et al., 2010) proposed the DP-warp (Deformable Projective warp) from the Generalized TPS warps and (Brunet et al., 2009) proposed the NURBS-warp (Non-Uniform-Rational-BSpline warp). Rational basis warps are modeled in homogeneous coordinates and employs the 3D bending energy as the penalty. As the name suggests, the 3D bending energy is the extension of the bending energy (equation (5)) to 3 dimensions (Tanner, 2005), computed in this case from the 2D homogeneous coordinates. As we will show in our experiments, the rational warps are challenging to optimize due to the rational terms as well as their sensitivities to the hyperparameter. In contrast to the existing approaches we propose to change the penalizer, using the squared residual of Schwarzian equations ε_{se} which forms infinitesimally projective warps. In fact, if our penalizer is imposed to the limit, the estimated warp becomes an homography:

$$\lim_{\lambda \rightarrow \infty} \left(\arg \min_{\eta} \varepsilon_d[\eta] + \lambda \varepsilon_{se}[\eta] \right) \in \mathcal{H}(\mathbb{R}^2). \quad (7)$$

3 Background

Projective differential invariants have been studied in computer vision in a few previous papers (Åstrom, 1995; Lazebnik and Ponce, 2005). In (Lazebnik and Ponce, 2005), the authors propose local projective differential invariants of curves and surfaces whereas (Åstrom, 1995) focuses on non-algebraic planar curves. None of the previous papers employed these invariants in deformable 3D reconstruction. We now present the Schwarzian derivative, one of the most fundamental projective differential invariants. We start our discussion with the cross-ratio of 4 points in the projective line and 5 points in the projective plane. We then give the differential version of the cross-ratio in the projective line, leading to the 1D Schwarzian derivative.

3.1 The Cross-Ratio

We consider 4 points t_1, t_2, t_3, t_4 in the projective line \mathbb{RP}^1 . The cross-ratio on \mathbb{RP}^1 is defined by the following scalar $\phi(t_1, t_2, t_3, t_4) = \frac{(t_1 - t_3)(t_2 - t_4)}{(t_2 - t_3)(t_1 - t_4)}$. Homographic transformations in $\mathcal{H}(\mathbb{RP}^1)$ preserve the cross-ratio. This directly extends to 4 colinear points in the projective plane \mathbb{RP}^2 . For 5 non-colinear points in \mathbb{RP}^2 , one may select one point as the reference and compute 4 direction vectors with the remaining 4 points. A cross-ratio is obtained by replacing distances by inter-direction signed angles. By changing the reference point one obtains 2 independent cross-ratios for 5 points in the projective plane.

3.2 The 1D Schwarzian Derivative

An important projective differential invariant is the Schwarzian derivative (Ovsienko and Tabachnikov, 2009). We give its derivation as can be found in the literature. We consider a diffeomorphism η which acts on 4 points $t_1, t_2, t_3, t_4 \in \mathbb{RP}^1$. We assume that the 4 points are spread so that t_2, t_3, t_4 can be defined by their distances to t_1 as a function of $\epsilon \in \mathbb{R}$: $t_2 = t_1 + \epsilon$, $t_3 = t_1 + 2\epsilon$ and $t_4 = t_1 + 3\epsilon$. The 4 points become $t_1, t_1 + \epsilon, t_1 + 2\epsilon, t_1 + 3\epsilon$ and thus are related by the variable ϵ . The Schwarzian derivative measures the effect of η on the cross-ratio as ϵ tends to zero. In other words, the Schwarzian derivative measures the cross-ratio of the points when they are infinitesimally close. To obtain the Schwarzian derivative one forms the Taylor expansion of ϕ when ϵ goes to zero and keeps the first non-zero term of the expansion:

$$\phi(\eta(t_1), \eta(t_2), \eta(t_3), \eta(t_4)) = \phi(t_1, t_2, t_3, t_4) - \epsilon^2 S[\eta](t_1) + O(\epsilon^3). \quad (8)$$

In the above equation $S[\eta]$ is the Schwarzian derivative in \mathbb{RP}^1 , defined by:

$$S[\eta] = \frac{\eta'''}{\eta'} - \frac{3}{2} \left(\frac{\eta''}{\eta'} \right)^2. \quad (9)$$

We can make two interesting observations: 1) the cross-ratio does not change in the first-order of ϵ and 2) despite being in the second-order of ϵ , the Schwarzian derivative is a third-order differential equation in η . The Schwarzian derivative $S[\eta]$ has some remarkable properties. From equation (8) it is easy to see that if $\eta \in \mathcal{H}(\mathbb{RP}^1)$, $S[\eta] = 0$ as the cross-ratio is then preserved by η . Conversely, it can be proved that $S[\eta] = 0$ implies that $\eta \in \mathcal{H}(\mathbb{RP}^1)$ (Ovsienko and Tabachnikov, 2005). Therefore, homographies are the only solutions of the differential equation $S[\eta] = 0$. With the Schwarzian derivative one can thus measure how close η is to a homography infinitesimally. Unfortunately, this derivation of the Schwarzian derivative in \mathbb{RP}^1 does not extend to \mathbb{RP}^2 .

3.3 Multidimensional Schwarzian Derivatives (MSDs)

The original Schwarzian derivative was only defined in 1D (Cayley, 1880; Kummer, 1836). However, over the last few decades, mathematicians have extended it to higher dimensions. Examples of MSDs can be found for different groups of diffeomorphisms. (Oda, 1974) first defined an MSD for locally biholomorphic mappings. (Osgood and Stowe, 1992) proposed the conformal MSD whereas (Ovsienko, 1989) proposed the ‘Lagrangian Schwarzian’ for the group of symmetric matrices. The case of MSD for differential projective structures, which is the extension to higher dimensions of the 1D Schwarzian, has also been studied by several authors (Matsumoto et al., 1993; Molzon and Mortensen, 1996; Ovsienko and Tabachnikov, 2005).

They provide as a general result for MSDs the 1-cocycle, a non-linear differential operator that vanishes for homographies. The 1-cocycle includes second order partial derivatives and rational terms. It cannot be used to ensure infinitesimally homographic warps as it also vanishes for other functions than homographies.

4 Schwarzian Equations in Two Dimensions

We propose the 2D Schwarzian equations, a system of PDEs with only homographies of \mathbb{RP}^2 as solutions. Unlike MSDs that are described by the 1-cocycle, we define the 2D Schwarzian equations as a set of PDEs where each member of the set vanishes for homographies. Interestingly, our Schwarzian equations in 2D are quadratic second order PDEs. This allows us to optimize the Schwarzp without using rational terms. We first show how to find the 1D Schwarzian derivative (9). We then use the same methodology to find the 2D Schwarzian equations.

4.1 The 1D Schwarzian Derivative

We define $\eta \in \mathcal{H}(\mathbb{RP}^1)$, formed by the ratio of two functions $\delta \in \mathcal{L}(\mathbb{R})$ and $\zeta \in \mathcal{L}(\mathbb{R})$. Our goal is to obtain the 1D Schwarzian derivative from the differential properties of η . To achieve that goal, we first proceed by multiplying η by its denominator ζ , obtaining:

$$\eta\zeta = \delta. \quad (10)$$

We then form second and third order derivatives of equation (10) to obtain the following two PDEs:

$$\eta''\zeta + 2\eta'\zeta' = 0 \quad (11)$$

$$\eta'''\zeta + 3\eta''\zeta' = 0, \quad (12)$$

where δ vanishes due to differentiation along with ζ'' . The next step is to eliminate ζ and ζ' from equations (11) and (12). We substitute the value of ζ' from equation (11) into equation (12) which cancels both ζ and ζ' and leads to:

$$\eta''' - \frac{3}{2} \frac{(\eta'')^2}{\eta'} = 0. \quad (13)$$

Dividing equation (13) by η' gives the 1D Schwarzian derivative as can be verified by direct comparison to equation (9). Multiplying equation (13) by η' , we arrive at the following third-order quadratic PDE:

$$\eta'\eta''' - \frac{3}{2}(\eta'')^2 = 0. \quad (14)$$

The main difference between equation (14) and the 1D Schwarzian derivative is that equation (14) does not have rational terms. Both of them have only homographies as solutions (see section 5). We call equation (14) the *1D Schwarzian equation*.

4.2 The 2D Schwarzian Equations

We propose a system of PDEs that represent the 2D Schwarzian equations. This system has by construction homographies as solutions.

We define function $\eta : (u, v)^\top \rightarrow (x, y)^\top \in \mathcal{H}(\mathbb{RP}^2)$:

$$\eta = \begin{pmatrix} \eta^x \\ \eta^y \end{pmatrix} \quad \text{with} \quad \eta^x = \frac{\delta^x}{\zeta}, \quad \eta^y = \frac{\delta^y}{\zeta} \quad \text{and} \quad \delta^x, \delta^y, \zeta \in \mathcal{L}(\mathbb{R}^2). \quad (15)$$

To obtain the Schwarzian derivatives in two dimension, as in the 1D case, we start by multiplying η^x and η^y by ζ and obtain the two following equations:

$$\eta^x \zeta = \delta^x \quad \text{and} \quad \eta^y \zeta = \delta^y. \quad (16)$$

By taking second order partial derivatives of equation (16) with respect to u and v we obtain the following 4 first-order PDEs:

$$\eta_u^x \zeta + \eta^x \zeta_u = \delta_u^x \quad \eta_u^y \zeta + \eta^y \zeta_u = \delta_u^y. \quad (17)$$

$$\eta_v^x \zeta + \eta^x \zeta_v = \delta_v^x \quad \eta_v^y \zeta + \eta^y \zeta_v = \delta_v^y. \quad (18)$$

We eliminate δ^x and δ^y by differentiating again equations (17) and (18) with respect to u and v , obtaining the following 6 second-order PDEs:

$$\eta_{uu}^x \zeta + 2\eta_u^x \zeta_u = 0 \quad \eta_{uu}^y \zeta + 2\eta_u^y \zeta_u = 0 \quad (19)$$

$$\eta_{vv}^x \zeta + 2\eta_v^x \zeta_v = 0 \quad \eta_{vv}^y \zeta + 2\eta_v^y \zeta_v = 0 \quad (20)$$

$$\eta_{uv}^x \zeta + \eta_u^x \zeta_v + \eta_v^x \zeta_u = 0 \quad \eta_{uv}^y \zeta + \eta_u^y \zeta_v + \eta_v^y \zeta_u = 0. \quad (21)$$

In these 6 PDEs, we have 3 terms (ζ_u , ζ_v and ζ) which we want to eliminate to obtain our 2D Schwarzian equations. By solving for ζ_u in equation (19), we find the first 2D Schwarzian equation:

$$\frac{\eta_{uu}^x \zeta}{2\eta_u^x} = \frac{\eta_{uu}^y \zeta}{2\eta_u^y} \quad (22)$$

$$\boxed{\eta_{uu}^x \eta_u^y - \eta_{uu}^y \eta_u^x = 0.} \quad (23)$$

Solving for ζ_v in equation (20) gives the second 2D Schwarzian equation:

$$\frac{\eta_{vv}^x \zeta}{2\eta_v^x} = \frac{\eta_{vv}^y \zeta}{2\eta_v^y} \quad (24)$$

$$\boxed{\eta_{vv}^x \eta_v^y - \eta_{vv}^y \eta_v^x = 0.} \quad (25)$$

Solving for ζ_v in equation (21) yields:

$$(\eta_{uv}^x \eta_u^y - \eta_{uv}^y \eta_u^x) \zeta + (\eta_v^x \eta_u^y - \eta_v^y \eta_u^x) \zeta_u = 0. \quad (26)$$

Multiplying the two equations in (19) by η_v^y and η_v^x respectively and subtracting them we obtain the following equation:

$$(\eta_{uu}^x \eta_v^y - \eta_{uu}^y \eta_v^x) \zeta - 2(\eta_v^x \eta_u^y - \eta_v^y \eta_u^x) \zeta_u = 0, \quad (27)$$

which we combine with equation (26) to cancel ζ_u , giving the third 2D Schwarzian equation:

$$\boxed{(\eta_{uu}^x \eta_v^y - \eta_{uu}^y \eta_v^x) + 2(\eta_{uv}^x \eta_u^y - \eta_{uv}^y \eta_u^x) = 0.} \quad (28)$$

In a similar way we obtain the fourth and last 2D Schwarzian equation by solving for ζ_u in equation (21) and combining the result with equation (20). The complete system of 4 2D Schwarzian equations is finally given by:

$$S_k[\eta] = 0, \quad \begin{cases} S_1[\eta] = \eta_{uu}^x \eta_u^y - \eta_{uu}^y \eta_u^x \\ S_2[\eta] = \eta_{vv}^x \eta_v^y - \eta_{vv}^y \eta_v^x \\ S_3[\eta] = (\eta_{uu}^x \eta_v^y - \eta_{uu}^y \eta_v^x) + 2(\eta_{uv}^x \eta_u^y - \eta_{uv}^y \eta_u^x) \\ S_4[\eta] = (\eta_{vv}^x \eta_u^y - \eta_{vv}^y \eta_u^x) + 2(\eta_{uv}^x \eta_v^y - \eta_{uv}^y \eta_v^x). \end{cases} \quad (29)$$

In contrast with the third-order 1D Schwarzian derivative, the 2D Schwarzian equations form a second-order quadratic system of PDEs. Obviously, the system in equation (29) is not unique. Any non-degenerate linear combination of these equations shares similar properties. This particular system naturally appears in the

proof of the next section.

5 Solution Space of the Schwarzian Equations

By construction, homographies are solutions of the Schwarzian equations (29). In this section, we prove that homographies are the *only* solutions. This proof builds the foundations of deformable surface modeling using Schwarzian equations in section 6. As in the previous section, we start with the 1D Schwarzian derivative and then extend the methodology to our 2D equations.

5.1 Solution Space of the 1D Schwarzian Derivative

We have proved in section 4 that by construction $S[\eta] = 0$ is a necessary condition for $\eta \in \mathcal{H}(\mathbb{RP}^1)$. The proof of the sufficient condition is outlined in (Ovsienko and Tabachnikov, 2005, chapter 1) yet we reproduce it in detail here as it helps us to introduce the proof in the 2D case.

Proposition 1: If $S[\eta] = 0$ then $\eta \in \mathcal{H}(\mathbb{RP}^1)$.

Proof. We proceed by showing that any $\eta \in \mathcal{C}^2(\mathbb{R}, \mathbb{R})$ can be expressed as the ratio of two linearly independent solutions of the following second order linear ODE with variable coefficients:

$$\varphi'' + \frac{1}{2}S[\eta]\varphi = 0. \quad (30)$$

As a consequence, if $S[\eta] = 0$, η is the ratio of solutions of $\varphi'' = 0$, which has linear functions as only solutions and thus implies that $\eta \in \mathcal{H}(\mathbb{RP}^1)$. We divide the proof in two main steps:

1. Find two functions φ_1 and φ_2 that satisfy the following three conditions: *i)* $\eta = \frac{\varphi_1}{\varphi_2}$, *ii)* φ_1 and φ_2 are linearly independent and *iii)* if $\eta \in \mathcal{H}(\mathbb{RP}^1)$ then $\varphi_1 \in \mathcal{L}(\mathbb{R})$ and $\varphi_2 \in \mathcal{L}(\mathbb{R})$.

To satisfy all aforementioned conditions we choose $\varphi_1 = \frac{\eta}{\sqrt{\eta'}}$ and $\varphi_2 = \frac{1}{\sqrt{\eta'}}$. *i)* is straightforward to check and *ii)* is satisfied given that $\varphi_1'\varphi_2 - \varphi_1\varphi_2' = 1$. To verify *iii)* we express $\eta \in \mathcal{H}(\mathbb{RP}^1)$ as the ratio of two functions $\delta \in \mathcal{L}(\mathbb{R})$ and $\gamma \in \mathcal{L}(\mathbb{R})$:

$$\delta = au + b \quad \gamma = cu + d, \quad (31)$$

where a , b , c and d are constant coefficients and thus η' can be expressed as

$$\eta' = \frac{\delta'\gamma - \delta\gamma'}{\gamma^2} = \frac{ad - cb}{\gamma^2}. \quad (32)$$

By substitution of equation (32) in the definition of φ_1 and φ_2 we verify that they are linear functions:

$$\varphi_1 = (ad - cb)^{-1}\delta \quad \varphi_2 = (ad - cb)^{-1}\gamma, \quad (33)$$

2. Find γ so that φ_1 and φ_2 are solutions of the following second order ODE with variable coefficients:

$$\varphi'' + \gamma\varphi = 0. \quad (34)$$

Equation (34) admits two linearly independent solutions and every solution is a linear combination of them (Coddington, 2012). To find γ we first substitute φ_1 in equation (34), obtaining the following expression:

$$\eta \left(\frac{3}{4}(\eta'')^2(\eta')^{-\frac{5}{2}} - \frac{1}{2}\eta'''(\eta')^{-\frac{3}{2}} \right) + \gamma\eta(\eta')^{-\frac{1}{2}} = 0. \quad (35)$$

By multiplying equation (35) by $\sqrt{\eta'}$ and grouping terms we obtain the following equation:

$$\eta \left(\gamma - \frac{1}{2}S[\eta] \right) = 0. \quad (36)$$

Similarly, if we substitute φ_2 in equation (34) it results in:

$$\gamma - \frac{1}{2}S[\eta] = 0. \quad (37)$$

For φ_1 and φ_2 to be solutions, we obtain from equations (36) and (37) that:

$$\gamma = \frac{1}{2}S[\eta]. \quad (38)$$

From equation (38), if $S[\eta] = 0$, then $\gamma = 0$ and φ_1 and φ_2 are two independent solutions of the ODE $\varphi'' = 0$, which admits only linear functions as solutions. As a consequence their ratio $\eta \in \mathcal{H}(\mathbb{RP}^1)$. ■

5.2 Solution Space of the 2D Schwarzian Equations

In the 2D case we found 4 Schwarzian equations S_1, \dots, S_4 . We have the function $\eta \in \mathcal{C}^2(\mathbb{R}^2, \mathbb{R}^2)$, where $\eta = (\eta^x, \eta^y)$ and we assume $J \neq 0$, where $J = \eta_u^x \eta_v^y - \eta_v^x \eta_u^y$ is the Jacobian determinant of η .

Proposition 2: If $S_k[\eta] = 0$ for $k \in \{1, 2, 3, 4\}$ then $\eta \in \mathcal{H}(\mathbb{RP}^2)$.

Proof. Similarly to the 1D case, we proceed by showing that any $\eta \in \mathcal{C}^2(\mathbb{R}^2, \mathbb{R}^2)$ can be expressed as ratios of

linearly independent solutions of the following second order system of linear PDEs with variable coefficients:

$$\varphi_{uu} + \alpha_1\varphi_u + \beta_1\varphi_v + \gamma_1\varphi = 0 \quad (39)$$

$$\varphi_{uv} + \alpha_2\varphi_u + \beta_2\varphi_v + \gamma_2\varphi = 0 \quad (40)$$

$$\varphi_{uu} + \alpha_3\varphi_u + \beta_3\varphi_v + \gamma_3\varphi = 0, \quad (41)$$

where we have that $\alpha_i = 0$, $\beta_i = 0$ and $\gamma_i = 0$ for $i \in \{1, 2, 3\}$ if $S_k[\eta] = 0$ for $k \in \{1, 2, 3, 4\}$. As a consequence, if the Schwarzian equations are satisfied, the only solutions of equations (39), (40) and (41) belong to $\mathcal{L}(\mathcal{R}^2)$ and thus $\eta \in \mathcal{H}(\mathbb{RP}^2)$. The proof involves two steps:

1. Find φ_1 , φ_2 and φ_3 that satisfy the following three conditions: *i)* $\eta_x = \frac{\varphi_1}{\varphi_3}$ and $\eta_y = \frac{\varphi_2}{\varphi_3}$, *ii)* φ_1 , φ_2 and φ_3 are linearly independent and *iii)* if $\eta \in \mathcal{H}(\mathbb{RP}^2)$ then $\varphi_j \in \mathcal{L}(\mathbb{R}^2)$ for $j \in \{1, 2, 3\}$.

The sought after functions are defined as follows:

$$\varphi_1 = \eta^x J^{-\frac{1}{3}} \quad \varphi_2 = \eta^y J^{-\frac{1}{3}} \quad \varphi_3 = J^{-\frac{1}{3}}. \quad (42)$$

From equation (42) *i)* is easily verified. To prove *ii)* we check that the Wronskian determinant of φ_1 , φ_2 and φ_3 is constant:

$$\begin{vmatrix} \varphi_{1,u} & \varphi_{1,v} & \varphi_1 \\ \varphi_{2,u} & \varphi_{2,v} & \varphi_2 \\ \varphi_{3,u} & \varphi_{3,v} & \varphi_3 \end{vmatrix} = 1, \quad (43)$$

where $\varphi_{i,u} = \frac{\partial \varphi_i}{\partial u}$ and $\varphi_{i,v} = \frac{\partial \varphi_i}{\partial v}$. Finally *iii)* can be easily checked by expressing η as a fraction of linear functions and verifying that in that case $J^{-\frac{1}{3}}$ is proportional to ζ , which makes φ_1 , φ_2 and φ_3 linear functions.

2. Find functions α_i , β_i and γ_i with $i \in \{1, 2, 3\}$ so that φ_1 , φ_2 and φ_3 are solutions of equations (39), (40) and (41). We proceed by substitution of equation (42) into equation (39), finding the following solution for the coefficients α_1 , β_1 and γ_1 :

$$\alpha_1 = \frac{S_3[\eta]}{3J} \quad \beta_1 = -\frac{S_1[\eta]}{J} \quad \gamma_1 = \frac{2}{J^2} \left(\frac{1}{9} S_3[\eta]^2 - \frac{1}{3} S_1[\eta] S_4[\eta] \right) - \alpha_{1,u} + \beta_{1,v}, \quad (44)$$

where $\alpha_{1,u} = \frac{\partial \alpha_1}{\partial u}$ and $\beta_{1,v} = \frac{\partial \beta_1}{\partial v}$. We repeat the same process for equations (40) and (41), obtaining

the rest of coefficients:

$$\alpha_2 = \frac{S_4[\eta]}{3J} \quad \beta_2 = \frac{S_3[\eta]}{3J} \quad \gamma_2 = \frac{1}{J^2} \left(-S_1[\eta]S_3[\eta] + \frac{1}{9}S_3[\eta]S_4[\eta] \right) - \alpha_{2,u} + \beta_{2,v} \quad (45)$$

$$\alpha_3 = \frac{S_2[\eta]}{J} \quad \beta_3 = \frac{S_4[\eta]}{3J} \quad \gamma_3 = \frac{2}{J^2} \left(\frac{1}{9}S_4[\eta]^2 - \frac{1}{3}S_2[\eta]S_3[\eta] \right) - \alpha_{3,u} + \beta_{3,v} \quad (46)$$

If $S_k[\eta] = 0$, for $k \in \{1, 2, 3, 4\}$, then from equations (44), (45) and (46) we have $\alpha_i = 0$, $\beta_i = 0$ and $\gamma_i = 0$ for $i \in \{1, 2, 3\}$. Therefore φ_1 , φ_2 and φ_3 are solutions of the following system of PDEs:

$$\varphi_{uu} = 0 \quad \varphi_{uv} = 0 \quad \varphi_{vv} = 0, \quad (47)$$

which has linear functions as only solutions and implies that $\eta \in \mathcal{H}(\mathbb{RP}^2)$. ■

6 Modeling the Perspective Projection of Deforming Surfaces: Swarps

The warp between two images of a plane is a homography. In that case, the 2D Schwarzian derivatives vanish, by definition. With a non-planar and possibly deforming surface, the image warp does not anymore satisfy the Schwarzian equations exactly. For a smooth surface deformation however, each small patch on the surface can be approximated by its tangent plane (see figure 2). The warp η can then be locally approximated by a homography between the projections of the tangent planes. The Schwarzian derivatives form differential invariants and we thus expect the system in equation (29) to have small residuals for the projection of infinitesimal planes.

For an image warp $\eta : \Omega_1 \rightarrow \Omega_2$, the 2D Schwarzian derivatives measure how near is η from a homography infinitesimally at each point. We define as Swarp a warp whose 2D Schwarzian derivatives were penalized for its estimation. As a result a Swarp captures differential projective properties.

A Swarp is defined as the solution of the following variational problem:

$$\arg \min_{\eta} \quad \epsilon_d[\eta] + \lambda \epsilon_{se}[\eta], \quad (48)$$

where $\epsilon_d[\eta]$ is a data term measuring registration error (for instance, the transfer error between point

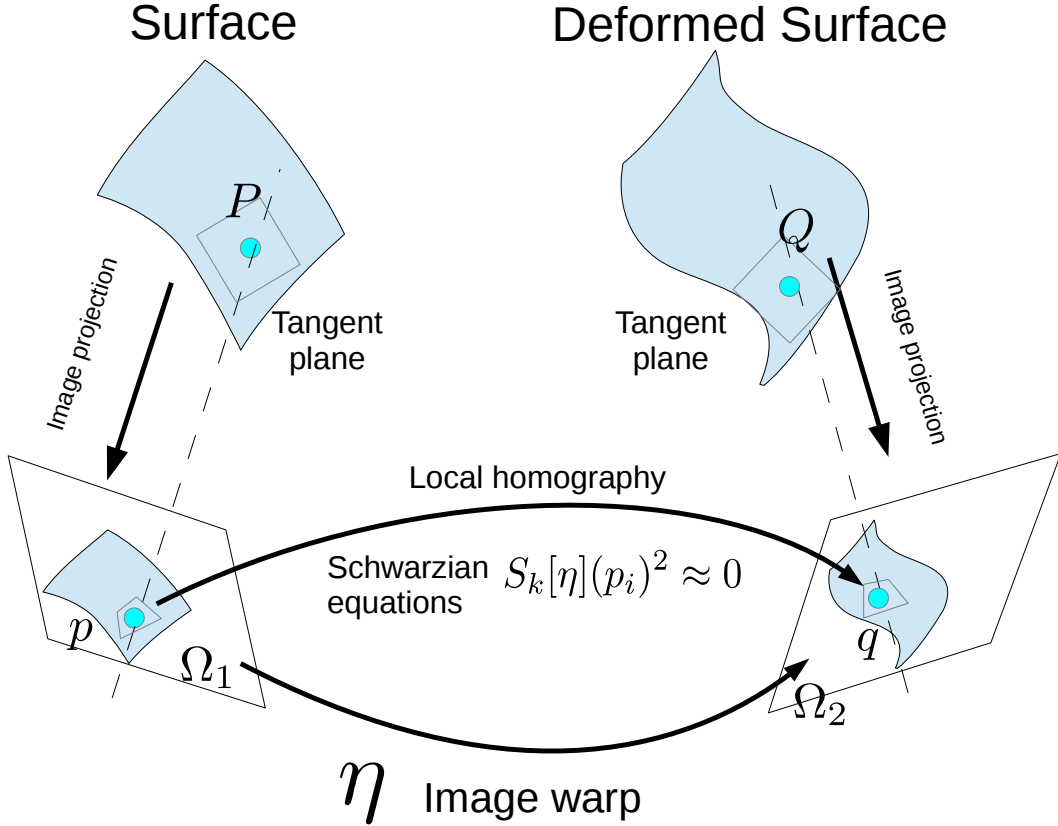


Figure 2: The 2D Schwarzian derivatives have small residuals for the warp η between the images of a smooth deforming surface.

correspondences), $\epsilon_{se}[\eta]$ is the Schwarzian penalty:

$$\epsilon_{se} = \int_{\Omega_1} (S_1[\eta]^2 + S_2[\eta]^2 + S_3[\eta]^2 + S_4[\eta]^2) d\Omega, \tag{49}$$

and λ is a hyperparameter which weighs the influence of the Schwarzian derivatives over the data term. In practice we replace the integral in equation (49) with a sum over a discretization $\tilde{\Omega}$ of the domain Ω :

$$\epsilon_{se} \approx \sum_{\mathbf{p}_i \in \tilde{\Omega}} \sum_{k=1}^4 S_k[\eta](\mathbf{p}_i)^2. \tag{50}$$

The Schwarzian penalty is quartic and non-convex. Solving the optimization problem (48) thus requires iterative optimization. We use the Levenberg-Marquardt algorithm. A Schwarp might be initialized with any warp (e.g. the BS-warp or the TPS-warp).

Name	Penalizer	Non-linear optimization	Initialized by
BS-warp	Bending Energy	No	N/A
BS-Schwarp	Schwarzian Equations	Yes	BS-warp
TPS-warp	Bending Energy	No	N/A
DP-warp	3D Bending Energy	Yes	TPS-warp
NURBS-warp	3D Bending Energy	Yes	BS-warp

Table 1: Summary of warps used in our experiments.

7 Experimental Results

We compare BS-Schwarp to state of the art warps, namely the BS-warp (Rueckert et al., 1999), the TPS-warp (Bookstein, 1989), the DP-warp (Bartoli et al., 2010) and the NURBS-warp (Brunet et al., 2009). In table 1 we summarize the details of warps used in our experiments. All these warp models are based on a set of control centers.

7.1 Implementation Details

For the experiments with synthetic data, we generate a set of 100 images for each configuration while varying imaging conditions (pose and focal length) and present the average values for each of the criteria over the 100 images. We keep the resolution of the images at 640×480 pixels. We vary the focal length between 100 and 500 pixels. We fix the number of feature correspondences to 50, control centers to 36 and use a Gaussian noise distribution (we vary the amount of noise for the same distribution). For all the other warps we use code publicly available from their authors.

7.2 Synthetic Data

We simulate images of rigid and deformable surfaces. In the rigid case, we use a plane and in the deformable case we wrap a surface around a longitudinal cut of a barrel. For both types of data, we examine the performance of all the warps against an increasing amount of noise, perspective and their sensitivity to their hyperparameter. In the deformable case, we add an additional experiment to compare the warps against an increasing amount of deformation. For all cases, we compare the warps based on three criteria: generalization error (ϵ_1), first derivative error (ϵ_2) and second derivative error (ϵ_3). The generalization error is the transfer error measured in terms of RMSR (Root Mean Square Residual) between the warp and ground truth. This is computed over some points which were not used to estimate the warps. We give a relative error for the first and second derivatives compared to ground truth.

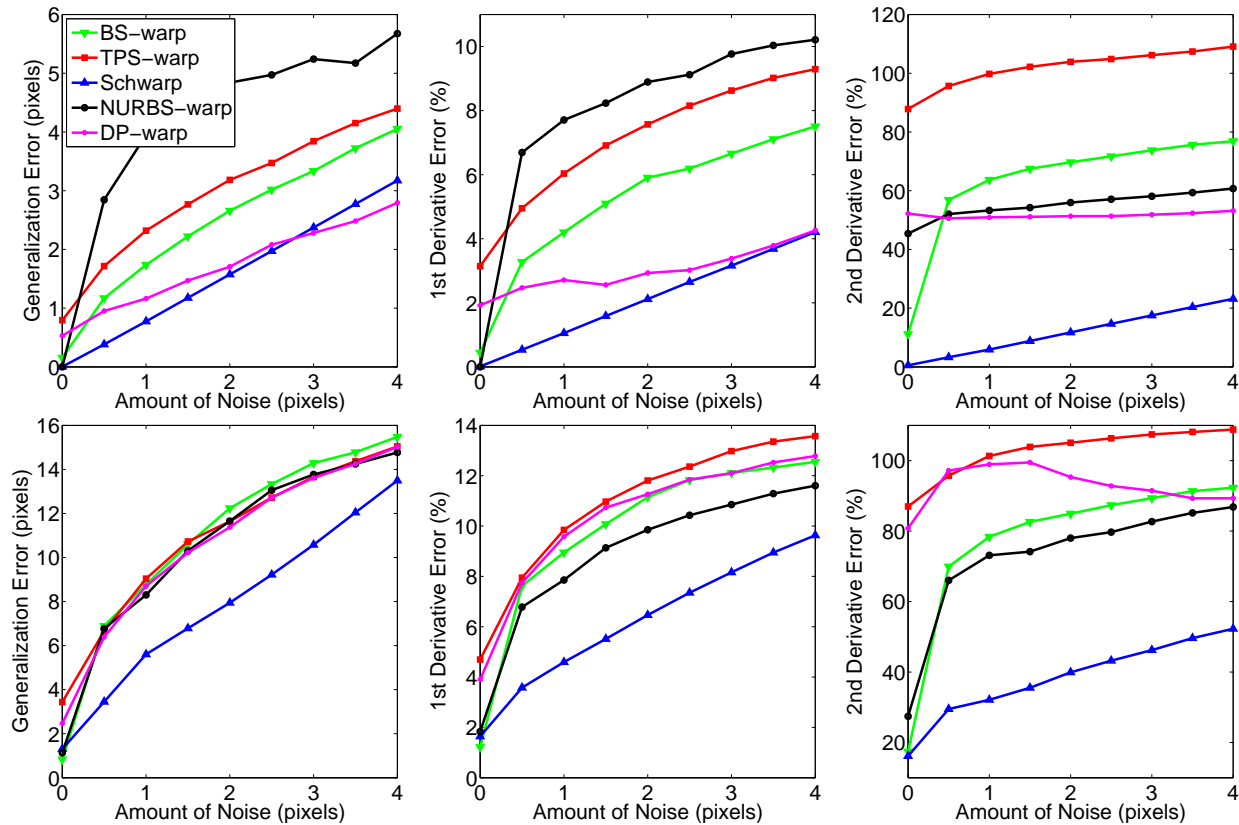


Figure 3: Comparison of BS-Schwarp with other warps against noise on synthetically generated images. The first and second rows are for the planar and deformable surfaces respectively.

7.2.1 Effect of Noise and Hyperparameter

We compute the warps with an increasing amount of noise and optimize the hyperparameter such that the generalization error is minimum in each case. Figure 3 presents the performance of all the warps against noise. In these experiments, the BS-Schwarp outperforms all the other warps in all criteria examined. This is true for both planar and deformable surfaces. As expected, the most significant improvement of the BS-Schwarp is in the case of second derivatives. The BS-Schwarp does not penalize the bending energy and thus preserves the second derivatives much better than any other warp that penalizes the bending energy. It is because, the bending energy directly penalizes the warp’s second derivatives.

To measure the sensitivities of the warps against the hyperparameter, we re-compute all the warps as in the previous experiment. However, this time we do not optimize the hyperparameter in each case. Instead, we use the mean of the optimal hyperparameter of an image for all different noise levels. This gives us 5 curves as in figure 3 but with larger errors since the hyperparameter is suboptimal for each case. For a given warp, the area between this new curve and the corresponding one in Figure 3 gives an estimate on a warp’s sensitivity to its hyperparameter. If this area is large, the warp is very sensitive to the hyperparameter. In table 2, we present the area between the two curves (with optimal and average hyperparameter) for all

Method	Planar Case			Deformable Case		
	ϵ_1	ϵ_2	ϵ_3	ϵ_1	ϵ_2	ϵ_3
BS-warp	2.3948	0.0566	0.4630	10.2054	0.1172	0.4537
BS-Schwarp	0.0275	0.0006	0.0025	3.6637	0.0329	0.1098
TPS-warp	2.0912	0.0470	0.1830	9.5280	0.0791	0.1895
DP-warp	10.1772	0.3194	1.2826	47.7706	0.1858	0.3079
NURBS-warp	0.4227	0.0216	0.3859	5.7904	0.1151	0.7170

Table 2: Sensitivities of the warps to their hyperparameter. The larger the number the more sensitive the warp to its hyperparameter.

warps for the planar and deformable cases. It is clear from these results that the BS-Schwarp is the most stable against its hyperparameter. In all cases, it undergoes the smallest deviation from the optimal curve.

7.2.2 Effect of Perspective

We compare the warps with a set of images with increasing perspective. To control the amount of perspective, we follow a single parameter projection model that allows us to select the amount of perspective required. With this model, a point $P = (P_x \ P_y \ P_z)^\top$ is projected as:

$$\Pi_t(P) = \left((t+1)f \frac{P_x}{P_z + tf} \quad (t+1)f \frac{P_y}{P_z + tf} \right)^\top. \quad (51)$$

Equation (51) becomes an orthographic projection for $t \rightarrow \infty$. Figure 4 shows that BS-Schwarp outperforms all the other warps with a significant margin. The errors increase linearly first, and then quadratically, with increasing perspective. It is interesting to note that BS-Schwarp models perspective better than the rational warps (DP-warp and NURBS-warp).

7.2.3 Effect of Deformation

We examine the behavior of the warps with an increasing amount of deformation (figure 5). Deformation is controlled by changing the radius of the curved surface. We can see a similar trend in this case: BS-Schwarp performs better than all the other warps. The generalization error and the first and second derivatives error degrade linearly with increasing deformation.

7.2.4 Rate of Convergence

In all experiments, we kept track of the number of iterations required for the non-linear refinement part of BS-Schwarp, DP-warp and NURBS-warp to converge to a solution. Indeed these 3 warps use Levenberg-Marquardt for their estimation. We have found that on average the BS-Schwarp takes only 10-15 iterations to converge, whereas the DP-warp and the NURBS-warp require hundreds of iterations. This indicates that

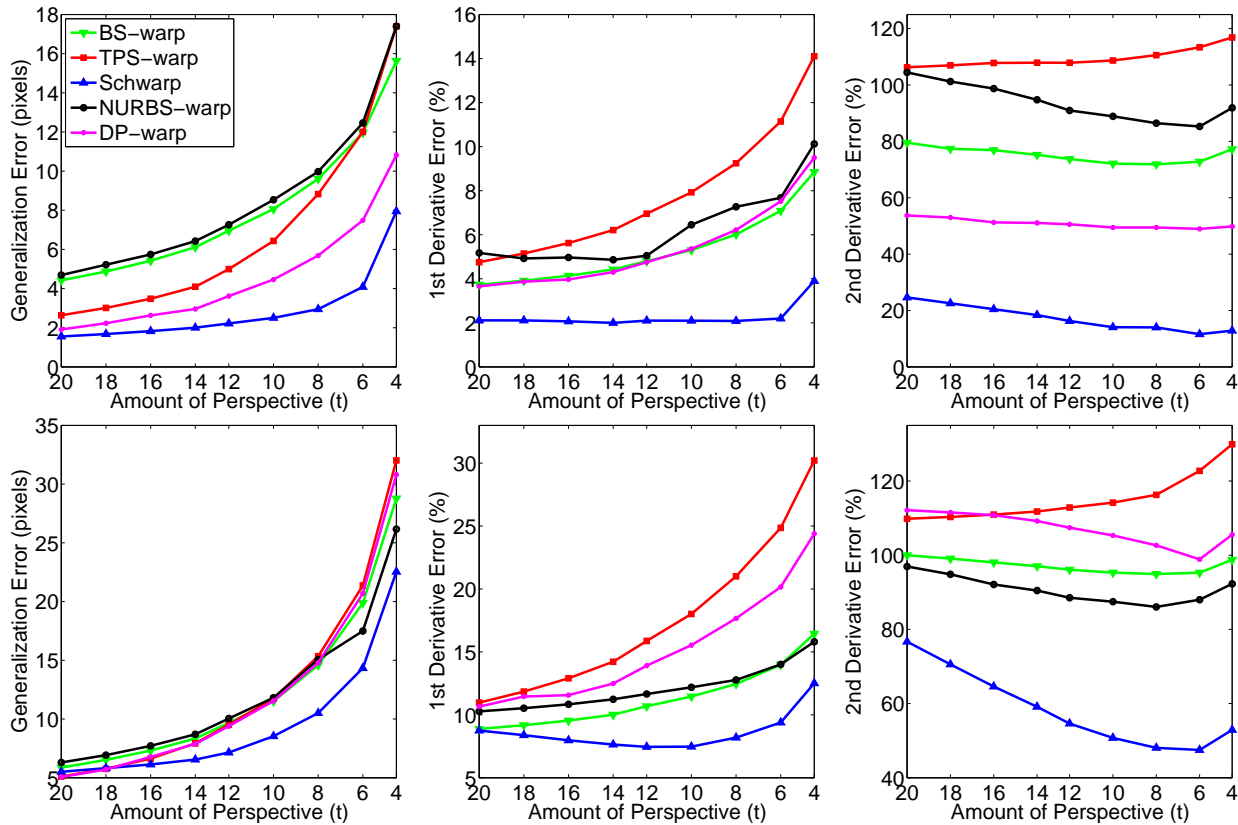


Figure 4: Performance of the different warps against increasing amount of perspective. The first and second rows are for planar and deformable surfaces respectively.

the BS-Schwerp is more stable numerically. This is due to the rational modeling of the DP-warp and the NURBS-warp.

7.3 Real Data

We compare the performance of the warps in three deformable reconstruction method on real images. The first two methods are based on SfT which uses the first derivatives of the warp, on the other hand, the third method (NRSfM) uses the second derivatives of the warp. Thus, these methods are able to provide a good idea of the impact of the quality of the warps. In figure 6, 7 and 8, we present the datasets used in the experiments. The resolutions of these images are 3264×4928 pixels. The focal length is 2448 pixels. For all the datasets, we obtain the ground truth shape Ψ using SfM.

We use different types of surfaces in our experiments. We deform these surfaces on several occasions and capture images of those deformations. The first dataset $D1$ consists of 8 different images of a deformable surface ($210\text{mm} \times 297\text{mm}$) which has texture all over it. This dataset allows us to examine the performances of the warps in the case where we have abundance of feature correspondences. The second dataset $D2$ consists of 7 images of another deformable surface of similar size as $D1$. However, it is textured only along the borders. This dataset is used to analyze the performance of the warps in cases where there are fewer or

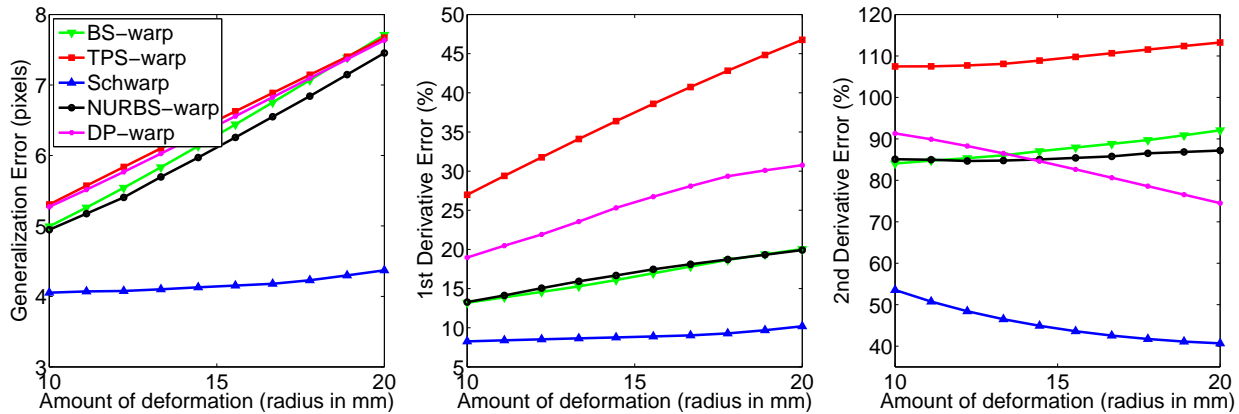


Figure 5: Performance of different warps against increasing amount of deformation.

no correspondences present in a part of the surface. The final dataset $D3$ is made of 6 images of another surface ($910\text{mm}\times 610\text{mm}$) which allows us to introduce an important perspective effect in the image thanks to its size. In each case, the best performing method’s results are shown in bold in the summary tables.

7.3.1 Shape Reconstruction in Shape-from-Template

In SfT, the shape of a surface is inferred from the warp computed between a template (typically an image of the flattened surface) and the image of the deformed surface. We use feature based approach to SfT (Bartoli et al., 2012). We use the SIFT (Lowe, 2004) feature detector to extract matches between the template and the target image and use the matches to compute the warp. Table 3 shows the reconstruction errors in SfT for each warps for all 3 datasets. The reconstruction error is computed between the reconstructed shape Ψ' and Ψ , using $\sum_{i,j\in\tilde{\Omega}} |\Psi'_{i,j} - \Psi_{i,j}|$, where $\tilde{\Omega}$ is the discretization of the domain. The errors are given in millimeters. The mean error for each dataset is also presented. From the results, it is clear that BS-Schwarp outperforms the other warps for each dataset. After BS-Schwarp, the second best performance is shared by the BS-warp in $D1$, the DP-warp in $D2$ and the NURBS-warp in $D3$. On average, BS-Schwarp improves the second best by 13.47% for $D1$, 3.59% for $D2$ and 12.12% for $D3$.

7.3.2 Calibration in Shape-from-Template

Calibration in SfT allows one to compute the focal length of the camera from the warp. We implemented the method proposed in (Bartoli and Collins, 2013b). We use all the computed warps for all the real images to recover the focal length (\hat{f}). We compute the relative error from the true focal length f , using $\frac{|\hat{f}-f|}{f}$. The results are presented in table 4. Here again, BS-Schwarp on average performs best for each dataset among all the warps. For more than half of the images, BS-Schwarp provides a better performance than the other warps.



Figure 6: The first dataset $D1$ comprises 8 images of a fully textured surface.

7.3.3 Non-Rigid Structure-from-Motion

We have used the method proposed in (Varol et al., 2009) that assumes the surface to be piece-wise planar. Homographies are fitted to feature correspondences between pairs of images and then are decomposed to obtain the orientation of surface planes. The surface’s shape is then computed from the normal field generated by combining all normals obtained from every pair. All pairs from at least 3 images are needed. The main difficulty of (Varol et al., 2009) is how to compute the support set of correspondences for each homography. We deal with this by uniformly sampling points from the first image and then using the warp to generate the local support of each point from close neighbors.

For this experiment, we use the first 6 images from the first dataset $D1$ and the whole set from the other datasets. For a dataset, each time we choose 3 images. We obtain several possible combinations of such image triplets. We compute shape error for all the combinations and present the mean error for 5 image warps. The shape error is computed using the mean difference between reconstructed surface normals and the ground truth surface normals. In table 5, we present the results of our experiments. It is clear that BS-Schwarp outperforms all the other warps with a good margin for all datasets.



Figure 7: The second dataset $D2$ comprises 7 images of a surface with texture only along the border.

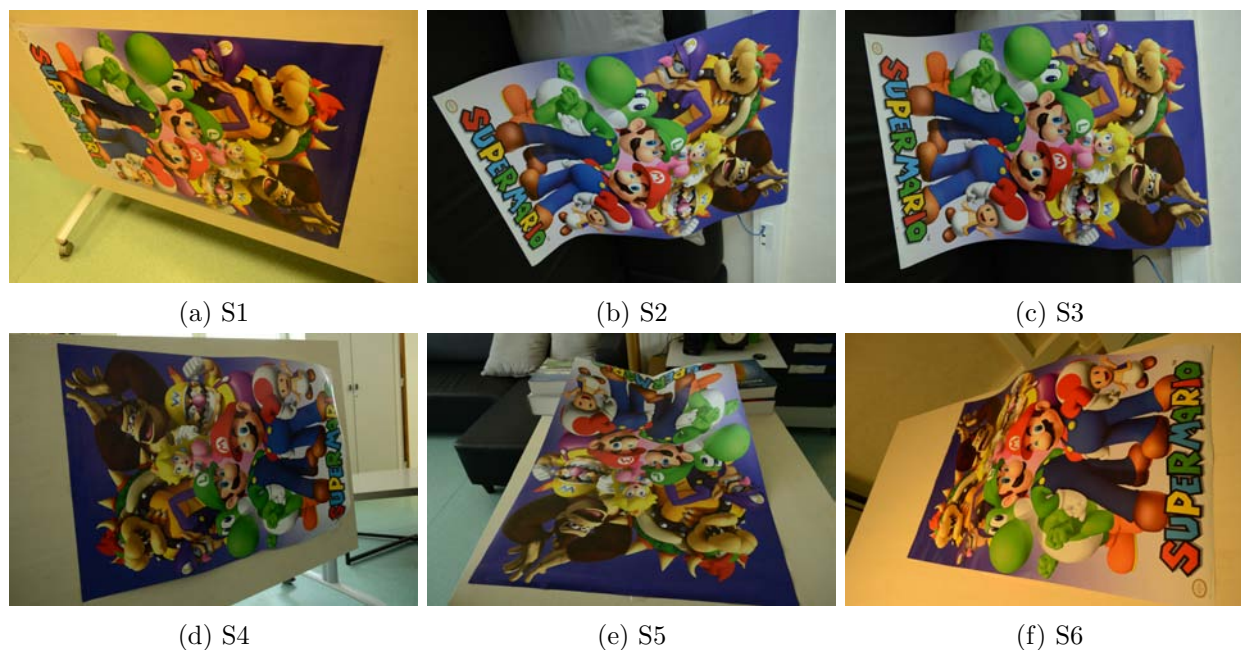


Figure 8: The third dataset $D3$ comprises 6 images of a fully textured surface larger than the surfaces used in $D1$ and $D2$.

Dataset	Shape	BS-warp	BS-Schwarp	TPS-warp	DP-warp	NURBS-warp
D1	S1	19.83	19.77	21.28	21.24	21.09
	S2	22.32	21.56	20.91	20.80	22.74
	S3	3.59	3.56	3.84	3.84	3.66
	S4	13.22	13.16	14.81	15.03	16.96
	S5	11.09	11.11	11.56	11.70	14.97
	S6	28.78	21.33	40.96	24.45	22.29
	S7	7.28	3.45	13.72	11.22	8.43
	S8	7.57	6.21	16.41	13.59	6.37
<i>D1-Mean</i>		<i>14.47</i>	<i>12.52</i>	<i>17.94</i>	<i>15.23</i>	<i>14.82</i>
D2	S1	14.61	14.57	15.12	15.20	14.67
	S2	9.04	9.01	11.30	10.72	15.76
	S3	12.45	12.44	13.43	13.26	12.98
	S4	11.70	11.81	12.17	11.93	11.37
	S5	18.88	12.36	43.78	13.07	12.25
	S5	28.78	21.33	40.96	24.45	22.29
	S6	43.91	41.64	42.76	42.52	48.39
	S7	20.13	20.47	20.41	20.24	20.82
<i>D2-Mean</i>		<i>18.67</i>	<i>17.48</i>	<i>22.71</i>	<i>18.13</i>	<i>19.60</i>
D3	S1	82.47	54.93	113.49	55.45	62.43
	S2	44.02	41.21	50.36	49.93	42.22
	S3	33.49	31.16	35.80	35.62	31.51
	S4	44.16	35.26	61.50	68.32	41.47
	S5	64.79	55.24	97.89	96.21	63.20
	S6	53.30	45.79	70.20	61.71	59.12
<i>D3-Mean</i>		<i>53.71</i>	<i>43.93</i>	<i>71.54</i>	<i>61.21</i>	<i>49.99</i>

Table 3: Reconstruction error (in mm) for SfT for the images of the 3 datasets used in our experiments.

8 Conclusion

We have studied differential projective invariants and their application for modeling the projection of a deforming surface. We have presented the 2D Schwarzian equations which form a set of PDEs. The Schwarzian equations model projective functions at a differential scale. They constrain the flow between two projections of a deforming surface. We have introduced a new type of penalty based on the warp’s Schwarzian equations. We have conducted experiments on real and simulated data. We show that the Schwarp (Schwarzian penalized warp) notably improves accuracy over the existing image warps (that penalize the bending energy) in SfT (shape reconstruction and calibration) and NRSfM. The Schwarzian equations provide a general model with potential impacts on other problems in computer vision (such as optical flow in rigid environments) which form potential future work.

Acknowledgments. This research has received funding from the EUs FP7 ERC research grant 307483 FLEXABLE.

Dataset	Shape	BS-warp	BS-Schwarp	TPS-warp	DP-warp	NURBS-warp
D1	S1	8.05	10.31	12.02	12.38	9.36
	S2	10.43	6.70	10.47	10.19	8.52
	S3	1.49	0.30	1.81	3.24	3.95
	S4	1.61	3.00	3.75	3.67	6.73
	S5	4.87	6.06	19.49	15.28	19.57
	S6	0.42	0.34	5.86	1.13	3.87
	S7	1.29	0.06	6.02	7.32	2.35
	S8	1.86	1.16	4.39	5.16	2.18
<i>D1-Mean</i>		<i>3.75</i>	<i>3.49</i>	<i>7.98</i>	<i>7.30</i>	<i>5.82</i>
D2	S1	3.00	0.85	2.01	0.02	0.10
	S2	3.12	1.41	8.09	8.05	8.64
	S3	12.45	11.58	7.25	8.01	19.61
	S4	4.99	4.15	4.67	4.07	3.08
	S5	0.50	0.46	19.61	2.88	6.22
	S6	19.85	19.81	19.77	19.85	19.77
	S7	2.05	4.71	14.96	9.64	2.48
<i>D2-Mean</i>		<i>6.51</i>	<i>6.14</i>	<i>10.91</i>	<i>7.5</i>	<i>8.56</i>
D3	S1	9.60	7.13	6.86	10.39	14.92
	S2	0.21	3.16	6.97	4.07	10.03
	S3	5.19	2.44	0.54	2.25	7.47
	S4	7.05	6.10	16.87	19.85	7.37
	S5	5.74	3.60	10.79	19.73	9.36
	S6	4.39	0.85	2.05	6.78	9.08
<i>D3-Mean</i>		<i>5.37</i>	<i>3.88</i>	<i>7.35</i>	<i>10.51</i>	<i>9.69</i>

Table 4: Relative focal length calibration recovery error (in percents) computed from the images of 3 datasets used in our experiments.

References

- K. Åström. Fundamental limitations on projective invariants of planar curves. *IEEE transactions on Pattern Analysis and Machine Intelligence*, 17(1):77–81, 1995.
- A. Bartoli and T. Collins. Template-based isometric deformable 3D reconstruction with sampling-based focal length self-calibration. In *Computer Vision and Pattern Recognition*, 2013a.
- A. Bartoli and T. Collins. Template-based isometric deformable 3D reconstruction with sampling-based focal length self-calibration. In *Computer Vision and Pattern Recognition*, 2013b.
- A. Bartoli, M. Perriollat, and S. Chambon. Generalized thin-plate spline warps. *International Journal of Computer Vision*, 88(1):85–110, 2010.
- A. Bartoli, Y. Gérard, F. Chadebecq, and T. Collins. On template-based reconstruction from a single view: Analytical solutions and proofs of well-posedness for developable, isometric and conformal surfaces. In *Computer Vision and Pattern Recognition*, 2012.

Dataset	Shape	BS-warp	BS-Schwarzp	TPS-warp	DP-warp	NURBS-warp
D1	S1	14.11	11.82	16.46	16.98	13.27
	S2	15.79	12.39	17.24	17.81	16.55
	S3	13.07	13.56	15.41	16.75	17.85
	S4	10.33	9.10	12.01	11.71	10.77
	S5	14.72	13.59	14.16	14.27	15.78
	S6	18.44	8.99	20.07	18.71	9.88
<i>D1-Mean</i>		<i>14.41</i>	<i>11.58</i>	<i>15.89</i>	<i>16.04</i>	<i>14.01</i>
D2	S1	14.22	10.90	19.70	14.91	10.68
	S2	8.07	7.05	12.09	10.14	11.56
	S3	8.06	6.84	11.98	8.69	7.62
	S4	7.72	6.12	9.98	8.51	7.53
	S5	7.44	3.80	23.19	6.21	4.45
	S6	11.02	12.71	14.85	14.43	13.36
	S7	10.03	9.35	15.44	13.21	11.04
<i>D2-Mean</i>		<i>9.54</i>	<i>8.11</i>	<i>15.32</i>	<i>10.87</i>	<i>9.46</i>
D3	S1	16.04	4.58	19.37	8.33	7.88
	S2	15.55	9.72	17.90	14.91	14.20
	S3	20.56	12.70	25.02	19.36	16.94
	S4	17.98	10.38	19.96	21.43	17.28
	S5	17.50	13.85	21.12	20.40	18.08
	S6	12.74	9.82	16.23	11.50	11.37
<i>D3-Mean</i>		<i>16.73</i>	<i>10.17</i>	<i>19.93</i>	<i>15.99</i>	<i>14.29</i>

Table 5: Shape recovery error (in degrees) comparison for NRSfM.

F. L. Bookstein. Principal warps: Thin-plate splines and the decomposition of deformations. *IEEE Transaction on Pattern Analysis Machine Intelligence*, 11(6):567–585, June 1989.

C. Bregler, A. Hertzmann, and H. Biermann. Recovering non-rigid 3D shape from image streams. In *Computer Vision and Pattern Recognition*, 2000.

F. Brunet, A. Bartoli, N. Navab, and R. Malgouyres. NURBS warps. In *British Machine Vision Conference*, 2009.

A. Cayley. On the Schwarzian derivatives and the polyhedral functions. *Transaction of Cambridge Philosophical Society*, 13, 1880.

E. A. Coddington. *An introduction to ordinary differential equations*. Courier Dover Publications, 2012.

O. D. Faugeras, Q.-T. Luong, and T. Papadopoulos. *The Geometry of Multiple Images: The Laws that Govern the Formation of Multiple Images of a Scene and Some of Their Applications*. MIT Press, 2001.

R. I. Hartley and A. Zisserman. *Multiple View Geometry in Computer Vision*. Cambridge University Press, ISBN: 0521623049, 2003.

- B. Horn and B. Schunck. Determining optical flow. *Artificial Intelligence*, 17:185–203, 1981.
- E. E. Kummer. Über die hypergeometrische reihe. *Journal Fur Die Reine Und Angewandte Mathematik*, 1836(15):39–83, 1836.
- S. Lazebnik and J. Ponce. The local projective shape of smooth surfaces and their outlines. *International Journal of Computer Vision*, 63:65–83, 2005.
- G. Lei. Recognition of planar objects in 3D space from single perspective views using cross ratio. *IEEE Transactions on Robotics and Automation*, 6(4):432–437, 1990.
- D. G. Lowe. Distinctive image features from scale-invariant keypoints. *International Journal of Computer Vision*, 60(2):91–110, 2004.
- K. Matsumoto, T. Sasaki, and M. Yoshida. Recent progress of Gauss-Schwartz theory and related geometric structures. *Memoirs of the faculty of Science, Kyushu University*, 47-2:283–381, 1993.
- R. Molzon and K. P. Mortensen. The Schwarzian derivative for maps between manifolds with complex projective connections. *Transactions of the American Mathematical Society*, 348(8):3015–3036, 1996.
- J. L. Mundy and A. Zisserman. *Geometric invariance in computer vision*. MIT Press, 1992.
- T. Oda. On schwarzian derivatives in several variables (in Japanese). *Kokyuroku Research Institute for Mathematical Sciences*, 226:82–85, 1974.
- B. Osgood and D. Stowe. The Schwarzian derivative and conformal mapping of Riemannian manifolds. *Duke Mathematical Journal*, 67(1):57–99, 1992.
- V. Ovsienko. Lagrange Schwarzian derivative. *Moscow University Mechanics Bulletin*, 44(6):8–13, 1989.
- V. Ovsienko and S. Tabachnikov. *Projective Differential Geometry Old and New: From the Schwarzian Derivative to the Cohomology of Diffeomorphism Groups*. Cambridge University Press, 2005.
- V. Ovsienko and S. Tabachnikov. What is... the Schwarzian derivative? *North American Mathematical Society*, 56:34–36, 2009.
- M. Perriollat, R. Hartley, and A. Bartoli. Monocular template-based reconstruction of inextensible surfaces. *International Journal of Computer Vision*, 95:124–137, 2011.
- J. Pilet, V. Lepetit, and P. Fua. Fast non-rigid surface detection, registration and realistic augmentation. *International Journal of Computer Vision*, 76(2):109–122, 2007.

- D. Rueckert, L. I. Sonoda, C. Hayes, D. L. G. Hill, M. O. Leach, and D. J. Hawkes. Nonrigid registration using free-form deformations: Application to breast MR images. *IEEE Transactions on Medical Imaging*, 18:712–721, 1999.
- M. Salzmann, J. Pilet, S. Ilic, and P. Fua. Surface deformation models for nonrigid 3D shape recovery. *Transactions on Pattern Analysis and Machine Intelligence*, 29(8):1481–1487, 2007.
- C. Schmid and A. Zisserman. The geometry and matching of lines and curves over multiple views. *International Journal of Computer Vision*, 40:199–233, 2000.
- D. Singer. Stable orbits and bifurcation of maps of the interval. *SIAM Journal of Applied Mathematics*, 35:2:260–267, 1978.
- R. Szeliski. Image alignment and stitching: A tutorial. *Foundations and Trends in Computer Graphics and Computer Vision*, 2(1):1–104, 2006.
- C. Tanner. *Registration and lesion classification of contrast-enhanced magnetic resonance breast images*. PhD thesis, University of London, 2005.
- P. Torr. MLESAC: A new robust estimator with application to estimating image geometry. *Computer Vision and Image Understanding*, 78:138–156, 2000.
- L. Torresani, A. Hertzmann, and C. Bregler. Non-rigid structure-from-motion: Estimating shape and motion with hierarchical priors. *IEEE Transactions on Pattern Analysis and Machine Intelligence.*, 30(5):878–892, 2008.
- A. Varol, M. Salzmann, E. Tola, and P. Fua. Template-free monocular reconstruction of deformable surfaces. In *International Conference on Computer Vision*, 2009.